PERGAMON

International Journal of Heat and Mass Transfer 46 (2003) 23–35

International Journal of HEAT and MASS TRANSFER

www.elsevier.com/locate/ijhmt

Effect of pressure, subcooling, and dissolved gas on pool boiling heat transfer from microporous, square pin-finned surfaces in FC-72

K.N. Rainey [a], S.M. You [b,*], S. Lee [c]

[a] Los Alamos National Laboratory, P.O. Box 1663, MS P940 Los Alamos, NM 87545-1663, USA

[b] Department of Mechanical and Aerospace Engineering, The University of Texas at Arlington, P.O. Box 19023, Arlington, TX 76019-0023, USA

[c] Intel Corporation, Desktop Architecture Lab, JF2-54, 2111 N.E. 25th Avenue, Hillsboro, OR 97124-5961, USA

Received 29 January 2002; received in revised form 30 June 2002

Abstract

The present research is an experimental study of the effects of pressure, subcooling, and non-condensable gas (air) on the pool nucleate boiling heat transfer performance of microporous enhanced finned surfaces. The test surfaces, solid copper blocks with 1-cm^2 bases and 5×5 square pin-fin arrays of 2, 4 and 8 mm fin lengths, were immersed in FC-72. The test conditions included an absolute pressure range of 30–150 kPa and a subcooling range of 0 (saturation) to 50 K. Effects of these parameters on nucleate boiling and critical heat flux (CHF) were investigated. In addition, differences between pure subcooled and gas-saturated conditions as well as horizontal and vertical base orientations were also investigated. Results showed that, in general, the effects of pressure and subcooling on both nucleate boiling and CHF were consistent with previously tested flat surface results, however, subcooling was found to significantly affect the high heat flux region of the microporous finned surfaces nucleate boiling curves. The relative enhancement of CHF from increased subcooling was greater for the microporous surface than the plain surface but less than a microporous flat surface. The horizontal orientation (horizontal base/vertical fins) was found to be slightly better than the vertical orientation (vertical base/horizontal fins). Correlations for both nucleate boiling and CHF for the microporous surfaces were also developed.

Keywords: Pool boiling; Enhancement; Fins; Pressure; Subcooling; Dissolved gas

1. Introduction

Recently, Rainey and You [1] showed that saturated nucleate boiling performance in FC-72 could be enhanced by employing a unique "double enhancement" technique: combining a large-scale area enhancement (square pin-fin array) and a small-scale surface enhancement (microporous coating). In order to develop reliable electronic cooling schemes utilizing boiling heat transfer and double enhancement, the effects of pressure, subcooling, and dissolved gas on the nucleate boiling heat transfer performance must be known.

The effects of pressure and liquid subcooling on the nucleate boiling performance of flat surfaces have been well studied in the literature. Increased pressure has been found to improve the nucleate boiling performance. Nishikawa et al. [2] attributed this behavior to an increased range of cavity radius that may be activated at a given wall superheat with increased pressure (increased active nucleation site density). As shown by Cichelli and

* Corresponding author. Tel.: +1-817-272-5635; fax: +1-817-272-2952.

E-mail addresses: rainey@lanl.gov (K.N. Rainey), you@uta.edu (S.M. You), seri.lee@intel.com (S. Lee).

0017-9310/03/$ - see front matter
PII: S0017-9310(02)00257-0

Nomenclature

a, b, c, d, e	constants
c_p	specific heat capacity (J/kg K)
g	gravitational acceleration (m/s^2)
h_{lv}	latent heat of vaporization (J/kg)
L	fin length (m)
q''	heat flux (W/m^2)
Ja	volumetric Jacob number, $Ja \equiv (\rho_l c_p \Delta T_{sub})/(\rho_v h_{lv})$
Pe	effective Péclet number, $Pe \equiv \sigma^{3/4}/(\alpha \rho_v^{1/2} \times (g(\rho_l - \rho_v))^{1/4})$
P	absolute pressure (kPa)
T	temperature (K)
ΔT_b	base surface superheat; $T_b - T_{sat}(P_{sys})$ (K)
ΔT_{sub}	liquid subcooling; $T_{sat}(P_{sys}) - T_{bulk}$ (K)
α	thermal diffusivity (m^2/s)
ρ	density (kg/m^3)
σ	surface tension (N/m)

Subscripts

b	base surface (area)
bulk	bulk liquid
CHF	critical heat flux
g	non-condensable gas (air)
l	saturated liquid
sat	saturated conditions
sub	subcooled conditions
sys	system or total
t	total surface area
v	saturated vapor
Z	CHF prediction of Zuber [12]

Bonilla [3] and others, the critical heat flux (CHF) will increase up to about one-third of the critical pressure and then decrease with increasing pressure. Subcooling has been found to have little or no effect on the fully developed nucleate boiling performance [4], however, CHF increases with increased subcooling showing a strong dependence [5,6]. Since the highly wetting fluids used in electronics cooling research can typically absorb large amounts of non-condensable gases (e.g. 48% by volume of air for FC-72 at standard conditions), the effects of dissolved gases on the boiling performance are also important to know. McAdams et al. [7] reported a strong enhancement of dissolved gas on the boiling curve at low heat fluxes (partially developed nucleate boiling) but only a weak effect at high heat fluxes (fully developed nucleate boiling). Watwe and Bar-Cohen [8] observed no effect of dissolved gas on CHF while Hong et al. [6] observed a dependence of CHF on dissolved gas only for small heaters when length-scale effects are significant.

The effect of pressure on the nucleate boiling and CHF performance of finned heaters appears to be consistent with flat heater observations [9–11]. In addition, Abuaf et al. [9] observed that the CHF for their flat and finned surfaces did not follow Zuber's [12] CHF correlation at very low pressures but leveled off with decreasing pressure instead. Mudawar and Anderson [13] studied the effects of subcooling on various cylindrical fin arrays in FC-72 at 1 atm. Except near CHF, their results showed insensitivity of the nucleate boiling curve to subcooling and found that they could dissipate up to 160 W/cm^2 with a subcooling of 35 K. To the author's knowledge, no studies have addressed the effects of dissolved gas on finned surfaces, however, Rainey and You's [1] observations of a dramatic change in the nucleate boiling curve slope of finned surfaces at high heat fluxes indicate that subcooling and/or dissolved gas may significantly affect the boiling performance in the high heat flux region.

The objective of the present work is to investigate the effects of pressure, subcooling, and dissolved gas (air) on the pool boiling heat transfer performance of microporous enhanced, pin-finned (double enhanced) surfaces and develop correlations for nucleate boiling and CHF. The surfaces are machined from solid copper, have a base surface area of 1 cm^2, and have a 5×5 square pin-fin array with fin lengths of 2, 4 and 8 mm. Testing is performed in FC-72 at 30, 60, 100 and 150 kPa absolute pressures and liquid subcoolings of 0 (saturated), 10, 30 and 50 K. In addition, comparisons are made between pure subcooled and gas-saturated conditions, horizontal and vertical orientations at 100 kPa, and plain and microporous coated finned surfaces. The microporous flat surface results from a companion study [14] are also included. The results of this study are intended to aid in the design of future electronic cooling schemes involving boiling heat transfer.

2. Experimental apparatus and procedure

2.1. Test facility

The pool boiling test facility used for the present work is the same as that used by Rainey and You [1], and is shown in Fig. 1. The main test chamber is a stainless steel pressure vessel with an internal water-cooled condenser, three band heaters located on the sides and bottom of the chamber, and an external temperature controller for bulk fluid temperature control. A

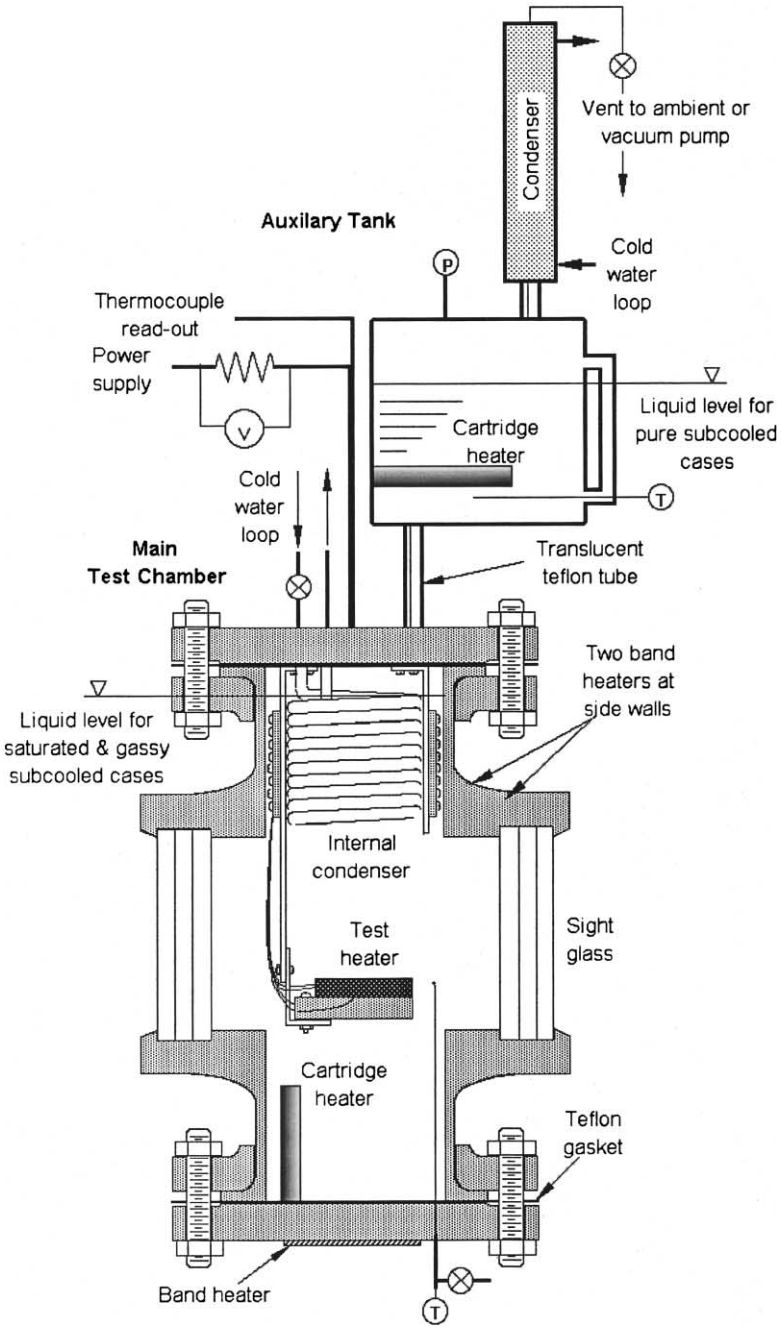

Fig. 1. Schematic of test apparatus.

cartridge heater was located in the bottom of the test chamber to provide additional heating/stirring during the degassing process. The auxiliary tank above the test vessel was used only for the pure subcooled testing to prevent regassing of the test liquid after degassing. An external condenser was used during degassing and atmospheric testing to prevent loss of test liquid. A pressure transducer located in the auxiliary tank was used to measure the internal gas pressure.

A computer controlled DC power supply was used to supply power to the test heaters. The heat flux supplied to the test heaters was determined from the measured voltage across the test heater and the current determined from the measured voltage across a shunt resistor. All

temperature, pressure, and voltage measurements were taken with a computer controlled data acquisition system.

2.2. Test heaters

The test heater design is identical to that of Rainey and You [1] and is shown in Fig. 2. The heating element is a two-layer thin metal film of tantalum and titanium nitride that has been sputtered onto a 0.5 mm thick silicon oxide coated silicon substrate along with copper for solder connections. The heating element was soldered to the copper block and copper tape power leads and had a total electrical resistance of about 20 Ω. The copper blocks were machined from solid pieces of copper using a high-speed steel slitting saw blade with a $10 \times 10 \times 2$ mm^3 base surface and 2, 4 and 8 mm fin lengths. The fins are square pin fins with a fin thickness of 1 mm and fin spacing of 1 mm in a 5×5 array as shown in Fig. 2. The copper block contained two thermocouple (type-T) wells centered in the base surface and spaced 5 mm apart and 5 mm deep. The copper/heater assembly was attached to a Teflon substrate using epoxy. The completed test heater was then mounted in a Lexan frame and surrounded by epoxy to generate a flush-mounted heating surface.

For the microporous coated test heater, the coating used is the ABM coating [15]. The microporous coating is a surface treatment technique used to increase vapor/gas entrapment volume and active nucleation site density by forming a porous structure of about 0.1–1 μm size cavities [15–18]. The ABM coating was named from the initial letters of its three components: 1–20 μm aluminum particles/devcon brushable ceramic epoxy/methyl-ethyl-ketone (MEK). The mixture of the three components was spray-coated over the finned surfaces using an airbrush. After the carrier (MEK) evaporates, the resulting layer consists of a microporous structure of aluminum particles and epoxy having a thickness of ≈50 μm. The microporous coating provides no significant increase of the heat transfer surface area.

2.3. Test procedure

The test fluid, FC-72, is a highly wetting dielectric perfluorocarbon produced by the 3M Industrial Chemical Products Division. FC-72 has been determined to be a good candidate fluid for immersion cooling applications because it is chemically stable/inert, dielectric, and has a relatively low boiling point ($T_{sat} = 56$ °C at atmospheric pressure). Prior to all testing, the test chamber was heated to the test liquid's saturation temperature using the three band heaters and the cartridge heater. Once at saturation temperature, the test liquid was boiled vigorously for at least 2 h to remove dissolved gases. Unless otherwise noted, test surfaces were tested in the horizontal, upward facing orientation. The test matrix consisted of studies on different subcooling and pressure conditions (Table 1).

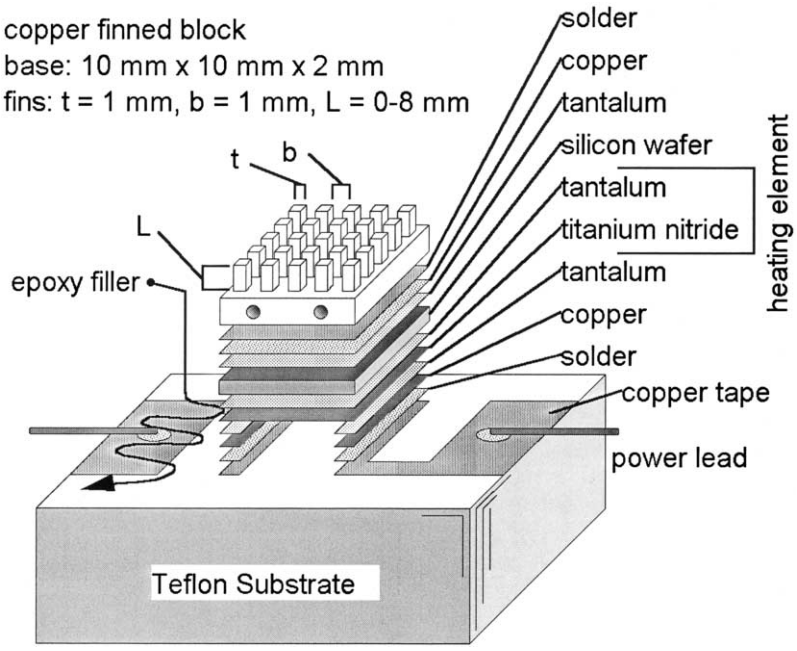

Fig. 2. Finned test heater design.

Table 1
Test matrix

Pressure, P_{sys} (kPa)	Liquid subcooling, ΔT_{sub} (K)			
	0 (sat.)	10	30	50
30	X[a]	X[a]	–	–
60	X[a]	X[a]	X[a]	–
100	X[b]	X[b]	X[b]	–
150	X[a]	X[a,c]	X[a,c]	X[a,c]

[a] Gas-saturated only.
[b] Both pure subcooled and gas-saturated.
[c] Microporous surface only.

2.4. Saturated cases

The fluid level for the saturation cases was maintained in the test chamber at about 15 cm above the test surface. After degassing, the external condenser was turned off. With the system still open to ambient, some of the test liquid was allowed to escape in order to push out any trapped air at the top of the condenser. After about 15 min, the valve at the top of the external condenser was closed. A vacuum pump was temporarily connected to the top of the external condenser to further make sure that all trapped air at the top of the condenser was removed. The measured temperature and pressure readings within the test chamber were checked against the FC-72 saturation curve to ensure that all non-condensables had been removed. The desired system pressure was then established by controlling the bulk fluid temperature using the internal condenser and three band heaters. After the desired pressure was obtained and stabilized, testing began. For the saturated tests at atmospheric pressure, a simpler procedure was used. Instead of the closed system approach above, the external condenser was left on and open to ambient (same procedure used by [1]).

2.5. Gas-saturated cases

The fluid level for the gas-saturated cases was maintained in the test chamber at about 15 cm above the test surface. After degassing, the external condenser was turned off and the valve at the top of the condenser was closed. The desired bulk fluid temperature was then established using the internal condenser and three band heaters. Once the desired temperature was obtained and stabilized, the valve at the top of the condenser was repeatedly cracked opened until the system stabilized at the desired pressure (the valve was then left closed during testing). This procedure produces a gas-saturated initial condition [19]. Although the gas content was not measured, it could be estimated from the relation $P_g = P_{sys} - P_v$, where P_{sys} is measured and $P_v = P_{sat}(T_{bulk})$. Testing then commenced. For the gas-saturated cases at atmospheric pressure, the external condenser was left on and open to ambient conditions.

2.6. Pure subcooled cases

In the present study, the pure subcooled testing was only performed at atmospheric pressure. The fluid level for the pure subcooled cases was maintained in the auxiliary tank at about 75 cm above the test surface. After degassing, the fluid in the auxiliary tank was maintained at saturation conditions for all of the pure subcooled testing to prevent regassing the subcooled fluid in the test chamber. With the system still open to ambient conditions, the desired bulk fluid temperature in the test chamber was then established using the internal condenser and three band heaters. Once the desired temperature was obtained and stabilized, testing began.

2.7. Boiling curves

After the proper fluid conditions were obtained and stabilized, two consecutive boiling curves were generated for each test surface. Identical boiling curves for each surface assured the consistency and repeatability of the data. There was a 2-h delay between runs to allow the heater and test section to return to steady state. Heat flux was controlled by voltage input. After each voltage change (heat flux increment), a 15-s delay was imposed before initiating data acquisition. After the delay, the computer repeatedly collected and averaged 125 base surface temperature measurements over 15 s until the temperature difference between two consecutive averaged temperature measurements for all thermocouples was <0.2 K. The test heater at this point was assumed to be at steady state. After reaching steady state, the heater surface and bulk fluid temperatures were measured and the heat flux was calculated. For heat flux values greater than $\approx 80\%$ of CHF, instantaneous surface temperature was monitored for 45 s after each increment to prevent heater burnout. Each instantaneous surface temperature measurement was compared with the previous steady-state surface temperature measurement. If a temperature difference larger than 20 K was detected, CHF was assumed and the power shut off. The CHF value was computed as the steady-state heat flux value just prior to power supply shutdown plus half of the increment.

2.8. Experimental uncertainty

Uncertainties for the heat flux and temperature measurements were estimated based on the method of Kline and McClintock [20]. Substrate conduction losses were estimated based on the values reported by O'Connor and You [16], whose heater had a similar

construction as the present one. Taking into account both measurement and substrate conduction errors, the uncertainty in heat flux (q''_b) was estimated as approximately 16% at 0.5 W/cm^2 and approximately 6% at 16, 80 and 120 W/cm^2. In addition, temperature measurement uncertainty was estimated considering thermocouple calibration error, temperature correction for the embedded thermocouples, and thermocouple resolution error. The uncertainty for temperature measurement was ± 0.4 K.

3. Results and discussion

The effects of pressure, subcooling, and dissolved gas (air) on the boiling heat transfer performance of microporous enhanced finned surfaces were investigated. The test surfaces were made from solid copper with 1-cm^2 (10×10 mm^2) base surfaces and fin lengths of 2, 4 and 8 mm and coated with the microporous coating. All testing was performed in FC-72 and under increasing heat flux conditions. For comparison, the microporous flat surface results from a companion study [14] are also included. Unless otherwise noted, all testing was performed with the test heaters in the horizontal, upward facing orientation (vertical fins). The fluid condition test matrix is listed in Table 1. The gas-saturated plain surface data at 150 kPa was not included in the present analysis due to excessive oxidation during testing which is discussed later.

3.1. Reference boiling curves

Fig. 3 illustrates the saturated nucleate boiling curves of the present plain and microporous finned surfaces at 100 kPa. For reference, the heat fluxes in Fig. 3 are based on the base area only and the wall superheats are calculated at the base of the fins. In addition, the single-phase portion of the boiling curves has been removed for clarity. The boiling curves of the 8 mm finned surfaces were stopped prior to CHF, so CHF values were not obtained for those cases. From Fig. 3, the effect of fin length on the plain surface boiling curves is clearly seen. As the fin length (area) increases, the boiling performance increases. Although not depicted, the present plain surface boiling curves were comparable to Rainey and You's [1] identically constructed plain surfaces. Rainey and You observed that the boiling performance of their plain finned surfaces increased proportionally with area up to fin lengths of 4 mm. Above this length, the performance degraded and was attributed to non-boiling fin tip conditions.

Also shown in Fig. 3 is the present microporous finned surface saturated boiling curves. As can be seen, the surface superheats of the microporous finned surfaces are significantly better than the plain surfaces. This

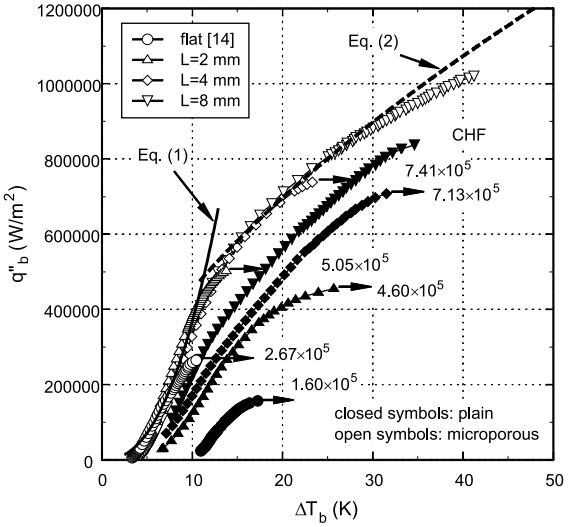

Fig. 3. Reference saturated boiling curves at 100 kPa.

shows the superior nucleate boiling performance of the microporous coated surfaces over plain surfaces, which has already been discussed in detail [15–17]. As previously reported by Rainey and You [1], the most striking feature of the microporous surface results is how the boiling curves collapse regardless of fin length unlike the plain surfaces in Fig. 3. Rainey and You attributed this to the increased availability of nucleation sites from the microporous coating. In addition, the lower wall superheats and decreased overall fin efficiencies [1] of the microporous finned surfaces may prevent the utilization of any additional surface area for a given base heat flux, q''_b.

Another interesting feature of the microporous surface results in Fig. 3 is the change in slope at about 500,000 W/m^2. Rainey and You [1] attributed this behavior to a temporal dry-out situation near the base of the fins caused by increased resistance on the re-wetting fluid from the fin geometry (increased blockage from the fins and bubble crowding). The present microporous finned surface boiling curves were also quite comparable to Rainey and You's results. Rainey and You's simple two line power-law curve fit given by:

$$q''_b = 1600\,\Delta T_b^{2.4} \quad \text{for } q''_b < 5 \times 10^5 \text{ W/m}^2 \tag{1}$$

$$q''_b = 1.08 \times 10^5\,\Delta T_b^{0.62} \quad \text{for } q''_b > 5 \times 10^5 \text{ W/m}^2 \tag{2}$$

is also shown in Fig. 3 for comparison. It can be seen from Fig. 3 that, although the nucleate boiling performance of the microporous surfaces is significantly increased over the plain surfaces, the CHF values are similar up to 4 mm fin lengths. Rainey and You attributed this lack of dependence of CHF on surface microstructure to the increased fluid re-wetting resistance

caused by the fin geometry. However, the CHF of the microporous 8 mm finned surface was much higher than the plain surface, which Rainey and You attributed to the microporous coating's better nucleation characteristics.

3.2. Effect of pressure

Fig. 4 illustrates the effect of system pressure on the saturated nucleate boiling curves of the microporous finned surfaces. The effect of pressure on the nucleate boiling performance is consistent with the prevailing trend in the literature of increased heat transfer coefficient with increased pressure [2,9–11] and appears to affect the entire boiling curve in the same manner. In general, the boiling curve slope appears to remain unchanged with increasing pressure. In addition, it is observed that pressure at saturated conditions does not affect the independence of the nucleate boiling curves to fin length. The CHF values (not shown in Fig. 4) show a significant increasing trend with increased pressure (discussed later), which is also consistent with the trends in the literature [3,9].

3.3. Effect of liquid subcooling

The subcooling level for the present work is defined as $\Delta T_{sub} = T_{sat}(P_{sys}) - T_{bulk}$, where P_{sys} equals the fluid vapor pressure, P_v, only for pure subcooled cases and the sum of fluid vapor and non-condensable gas partial pressures for gas-saturated cases or $P_{sys} = P_v + P_g$ [19]. Figs. 5–8 illustrate the effects of subcooling at all four tested system pressures for the microporous finned surfaces along with the flat microporous surface results from Rainey [14] for comparison. The single-phase convection data has been removed for clarity. In addition, the high heat flux portions of many of the boiling curves (especially in Fig. 8) are missing because the boiling curve tests were stopped when the base temperature reached or exceeded 100 °C. As discussed earlier, this was done to avoid decomposition of FC-72 onto the heater surfaces. In addition, for electronics cooling applications, maximum allowable case temperatures are usually below 100 °C, therefore, heat transfer performance information in the temperature range above

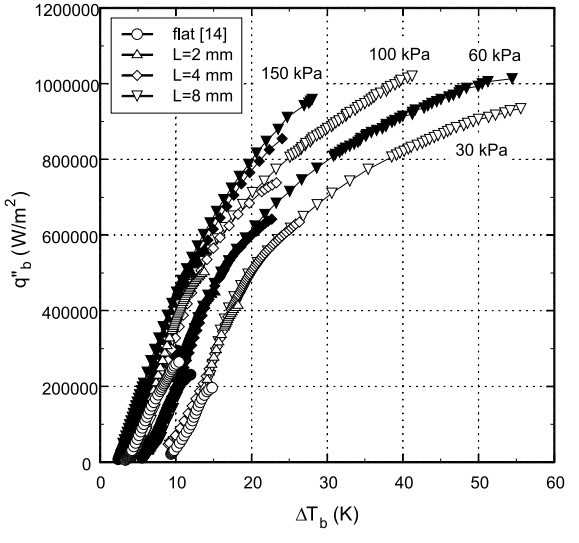

Fig. 4. Pressure effect for microporous saturated boiling curves.

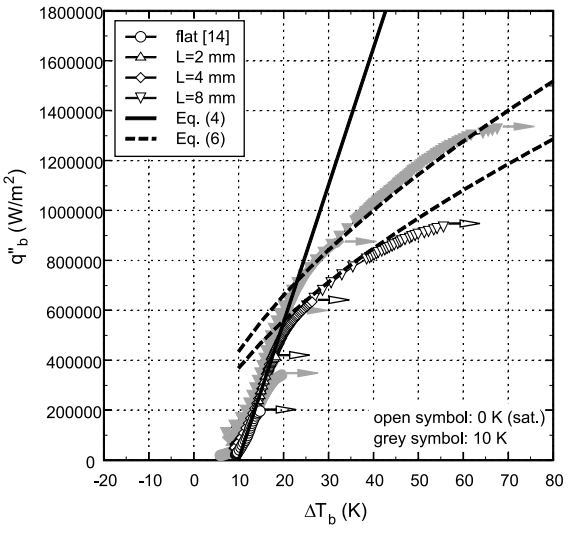

Fig. 5. Gas-saturated boiling curves of microporous surfaces at 30 kPa.

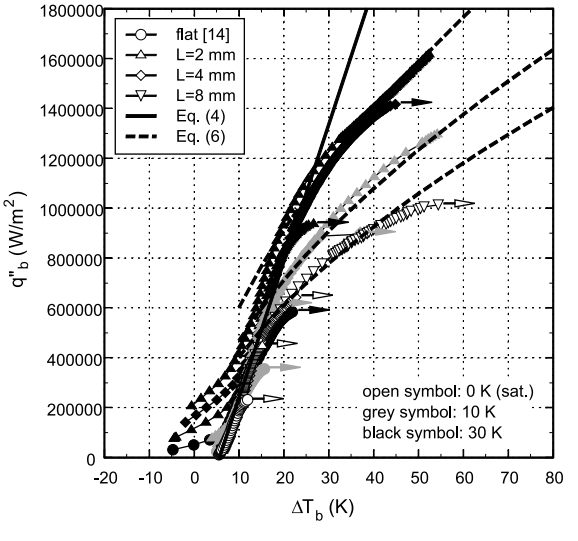

Fig. 6. Gas-saturated boiling curves of microporous surfaces at 60 kPa.

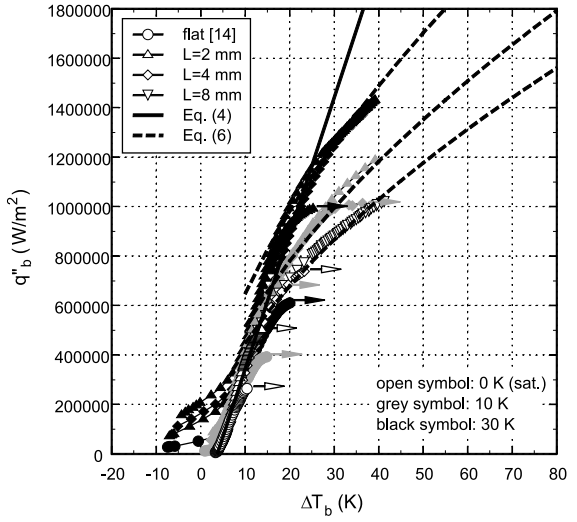

Fig. 7. Gas-saturated boiling curves of microporous surfaces at 100 kPa.

100 °C would not be very useful. The effects of subcooling on the microporous finned surfaces can be clearly seen in Figs. 5–8. In the low heat flux region, the nucleate boiling curves collapse to one line regardless of subcooling or fin length. The effect of the dissolved gas can be seen as an enhancement of the low heat flux boiling performance just after incipience, which is discussed later. Although the low heat flux region is unaffected, increasing the subcooling appears to shift the point at which the boiling curve slope changes which results in a dependency of the high heat flux region of the nucleate boiling curve on subcooling. The increased subcooling most likely decreases bubble crowding between the fins through bubble condensation and thus decreases the resistance to the re-wetting fluid which would delay the formation of localized temporal dry-out near the base of the fins and ultimately shift the high heat flux portion of the boiling curve upward.

3.4. Gas-saturated vs. pure subcooling

Before discussing the dissolved gas effect, some terminology needs to be clarified. The term "gas-saturated" is used in the present work to describe the initial condition of the fluid as being saturated with non-condensable gas (air). The term "gassy subcooled" is used in the present work to describe the fluid condition near the heater surface during boiling, which contains an indeterminable amount of dissolved gas; in other words, a condition that is somewhere between gas-saturated and pure subcooled. The term "pure subcooled" naturally refers to a completely degassed, subcooled fluid condition. In order to distinguish between subcooling and dissolved gas effects, Fig. 9 compares the pure subcooled and gas-saturated nucleate boiling curves of the 4 mm microporous finned surface at 100 kPa. The single-phase convection data has been removed for clarity. From Fig. 9, it can be seen that at low heat fluxes just after incipience, the dissolved air significantly enhances heat transfer but the effect diminishes with increasing heat flux similar to that observed for the flat surfaces from Rainey [14]. The initial boiling enhancement is attributed to a larger number of active nucleation sites from the gas partial pressure within the embryonic bubbles, faster bubble growth, and increased bubble wake con-

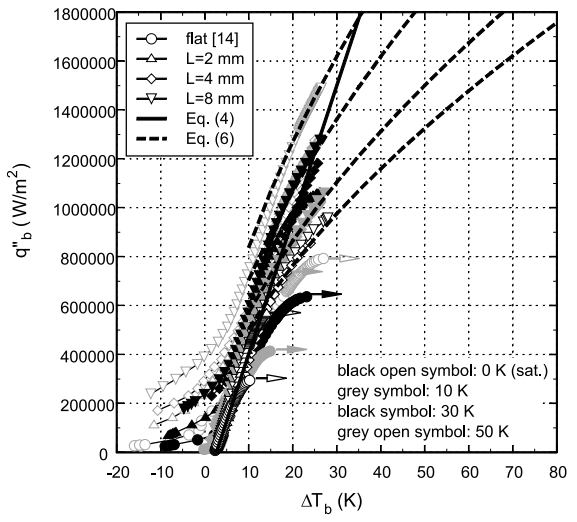

Fig. 8. Gas-saturated boiling curves of microporous surfaces at 150 kPa.

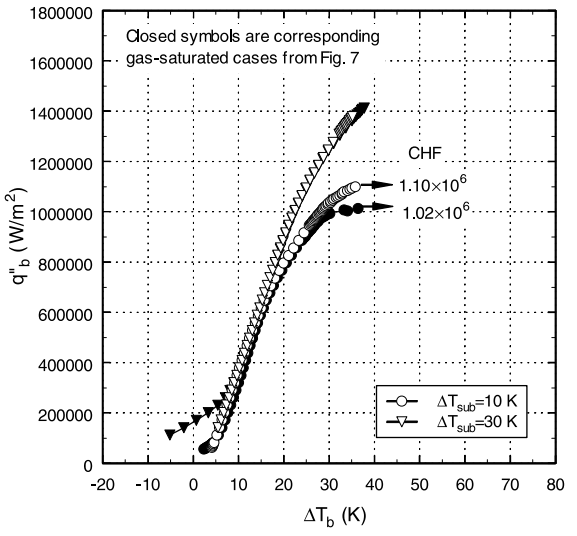

Fig. 9. Comparison of pure subcooled and gas-saturated boiling curves of the 4 mm finned microporous surface at 100 kPa.

vection [21] while the decrease in boiling enhancement with increased heat flux is attributed to depletion of the dissolved air near the heater surface creating a gassy subcooled condition [19]. This gas depletion also produces CHF values that are almost the same as the pure subcooled values as shown in Fig. 9. From Figs. 5–8, it can be seen that the boiling enhancement from the dissolved air increases with increasing pressure and subcooling. This is due to the increased dissolved air content as observed by You et al. [21] (the dissolved air content increases with increasing pressure and subcooling).

3.5. Effect of orientation

In addition to dissolved gas effects, the effect of heater orientation was also investigated. Fig. 10 compares the gas-saturated boiling curves of the 4 mm microporous finned surface at 0° (base is upward facing; fins are vertical) and 90° (base is vertical; fins are horizontal) inclinations. From Fig. 10 it is observed that the 90° boiling curves are slightly worse than 0° boiling curves. Although not shown, the 4 mm plain finned surface also showed this behavior. This may be due to decreased boiling effectiveness from the downward facing fin surfaces in the 90° orientation. Rainey and You [22] as well as many others have already shown that downward facing surfaces exhibit much worse boiling performance than vertical or horizontal surfaces. In contrast to the present results, both Kumagai et al. [23] and Guglielmini et al. [10] observed that heat transfer coefficients were generally better at the 90° orientations for their plain finned surfaces. The differences between the present results and those of Kumagai et al. and Guglielmini et al. may be due to differences in fin geometry. Both Kumagai et al. and Guglielmini et al. used smaller fin spacings than the present study, which could significantly affect the vapor removal behavior.

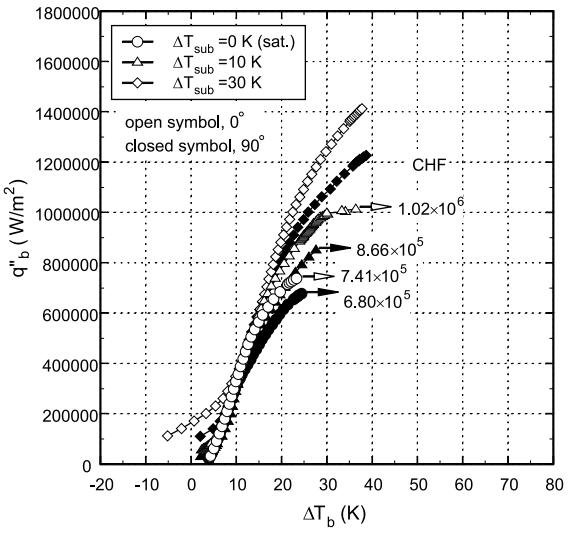

Fig. 10. Orientation effect on 4 mm finned microporous surface at 100 kPa (gas-saturated).

3.6. Correlation of nucleate boiling curves

From Rainey and You [1], the boiling curves of microporous finned surfaces were found to consist of a low and high heat flux region that required two separate correlations (Fig. 3). From the present results shown thus far, it is concluded that, for a given fluid within the present range of conditions, the low heat flux region of the microporous finned surfaces is essentially a function of pressure only while the high heat flux region is a function of pressure and subcooling. The authors found that the present low heat flux data are better correlated with a linear fit than Rohsenow's [24] power-law correlation. The reason for the failure of Rohsenow's correlation to adequately describe the present data may be due to length-scale/heater size effects; however, more study is needed before any conclusions can be made.

It was decided to correlate the present low heat flux region data in Figs. 5–8 with a linear equation in the following form:

$$q''_{\mathrm{b}} = a\,\Delta T_{\mathrm{b}} - bP^{c}_{\mathrm{sys}} \tag{3}$$

The constants a, b and c were determined by fitting the linear portions of the nucleate boiling data from Figs. 5–8. The heat flux data that was affected by the dissolved air were removed prior to fitting the data. The slope, a, in Eq. (3) was found by averaging the slopes of each individual boiling curve at all pressures except 150 kPa (the data at 150 kPa had too much scatter from dissolved gas effects). Once the slope was fixed, the y-intercepts were found for each pressure and correlated using a power-law fit. From this procedure, the present microporous surface saturated and gas-saturated low heat flux data are well correlated by the following equation:

$$q''_{\mathrm{b}} = 5.49 \times 10^{4}\,\Delta T_{\mathrm{b}} - 8.68 \times 10^{6} P^{-0.814}_{\mathrm{sys}} \tag{4}$$

Eq. (4) is plotted as a thick solid line in Figs. 5–8.

For the high heat flux region of the microporous surfaces, Rainey and You [1] used a power-law correlation:

$$q''_{\mathrm{b}} = \mathrm{d}\,\Delta T^{\mathrm{e}}_{\mathrm{b}} \tag{5}$$

The present microporous high heat flux data also fit this type of correlation, however, d in Eq. (5) is now a function of pressure and liquid subcooling. Prior to fitting the high heat flux region, the bending portion of the data near CHF was removed. After fitting each pressure and subcooling separately with Eq. (5) and then

combining the results, it was found that the data were well correlated with the following modified equation:

$$q''_b = (284P_{sys} + 1670\Delta T_{sub} + 84200)\Delta T_b^{0.6} \quad (6)$$

Eq. (6) is also plotted in Figs. 5–8 as thick dashed lines. As can be seen in Figs. 5–8, Eqs. (4) and (6) describe the effect of pressure and subcooling for the microporous surfaces in the present range of test conditions in FC-72 quite well.

3.7. Critical heat flux

The four parameters that were found to affect CHF in the present data are: pressure, subcooling, fin length, and surface microstructure (plain or microporous). With regard to the effects of pressure, Zuber's [12] correlation given by:

$$q''_{CHF,Z} = (\pi/24)h_{lv}\rho_v^{1/2}[g\sigma(\rho_l - \rho_v)]^{1/4} \quad (7)$$

has been found to predict the effects of pressure for flat surfaces in the present range of test conditions reasonably well [25,26]. For the analysis of CHF behavior, the present microporous surface CHF values (based on total surface area) were normalized by Eq. (7). Fig. 11 illustrates the microporous surface CHF behavior of the saturated cases for all fin lengths and pressures. The flat surface data of Rainey [14] and the 0.5 mm finned microporous surface saturated data of Rainey and You [1] have been added as well. From Fig. 11, it can be seen that the normalized CHF values decrease linearly with increasing fin length. Rainey and You's [1] microporous finned surface data also show this trend, although to a lesser degree. This is most likely caused by decreasing fin tip heat transfer effectiveness from reduced fin tip temperatures with increasing fin length. Between 0 (flat) and 2 mm fin lengths, the CHF performance drops significantly. Rainey and You [1] also observed this loss of enhancement from the microporous coating and attributed it to increased liquid re-wetting resistance from bubble crowding and fin blockage, which effectively removed the dependency of CHF on surface microstructure (for fin lengths of 4 mm and less). With regard to pressure, the 60–150 kPa results are comparable which suggests that Zuber's correlation predicts the effects of pressure in this range quite well, however, the 30 kPa results are significantly different. This indicates that Zuber's correlation does not predict the effects of pressure very well at low pressures, which has already been observed by Gorodov et al. [27] and Abuaf et al. [9]. As can be seen from Fig. 11, the CHF values of the microporous finned surfaces appear to be roughly linear with fin length in the range tested, therefore, for estimation purposes only, the 60–150 kPa finned surface CHF data in Fig. 13 were best fit as:

$$q''_{t,CHF,sat}/q''_{CHF,Z} = 1.23 - 51L \quad (8)$$

where

$$q''_{t,CHF,sat} = q''_{b,CHF,sat}/(1000L + 1) \quad (9)$$

With regard to the effects of subcooling on CHF, the authors found that Inoue et al.'s [28] correlation given by:

$$q''_{CHF,sub} = q''_{CHF,sat}\left[1 + 0.84(\rho_v/\rho_l)^{1/4}Ja/Pe^{1/4}\right] \quad (10)$$

fit the present data at all tested pressures quite well. The exponents on the density ratio and Pe in Eq. (10) for the microporous finned surfaces were found to match those of the flat surfaces from Rainey [14]. The constant of 0.84 in Eq. (10) was found to be independent of fin length for the range tested, however, it is reduced from the microporous flat surface value of 1.20 [14]. Fig. 12 illustrates the effects of subcooling on CHF for the microporous surfaces at all tested pressures. The denominator of the y-axis, $q''_{CHF,sat}$, is the individual saturated CHF value for each surface at the same system pressure. The flat surface results from Rainey [14] are included as well. As can be seen in Fig. 12, Eq. (10) correlates the present finned data quite well. The finned surfaces show less sensitivity to increased subcooling than the flat surfaces. As subcooling is increased, the resistance on the re-wetting fluid to the surface is expected to decrease because of decreased bubble crowding from increased bubble condensation. The finned surfaces may not experience as much enhancement from subcooling as the flat surface because of the additional blockage effects

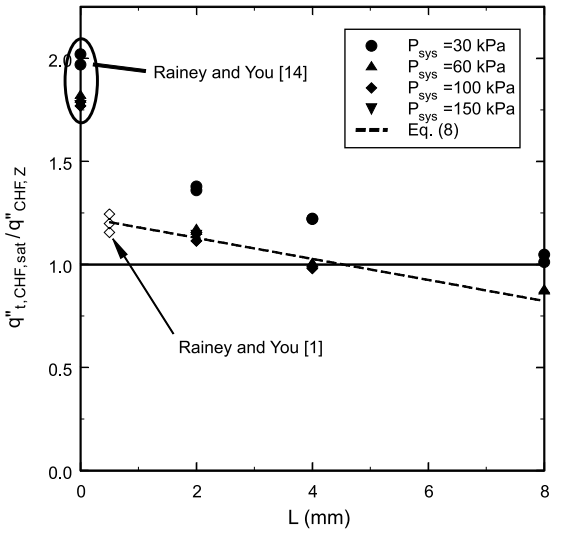

Fig. 11. Effect of pressure and fin length on saturated CHF for microporous surfaces.

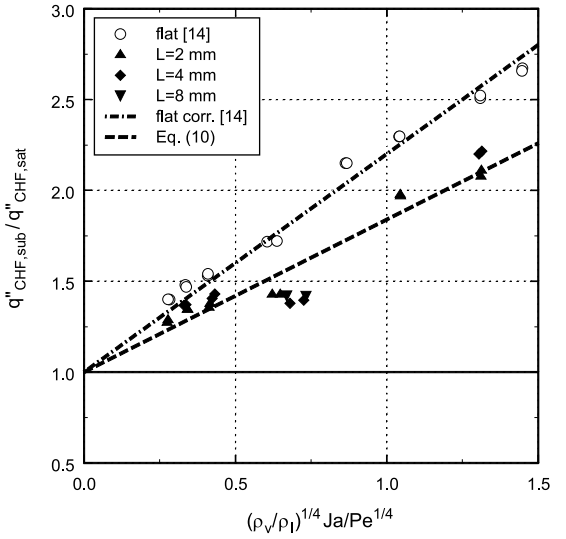

Fig. 12. Effect of subcooling on CHF for microporous surfaces (gas-saturated).

from fin geometry, which is unaffected by subcooling (smaller relative change in apparent flow area for the re-wetting fluid).

3.8. Plain surface results

Testing was also performed on plain finned surfaces. Fig. 3 shows the saturated boiling curves for all fin lengths at 100 kPa while Fig. 13 compares the effects of subcooling/dissolved gas at 100 kPa for the 4 mm plain and microporous finned surfaces. The single-phase convection data has been removed for clarity. In general, the plain surfaces showed similar behavior to pressure and subcooling with the microporous surfaces, however, there are a few notable differences. Unlike the microporous finned surfaces, most of the plain finned surfaces' nucleate boiling curves were affected by increased subcooling as can be seen in Fig. 13. Excessive oxidation of the plain copper surfaces occurred at the 150 kPa gas-saturated conditions (high dissolved gas content), which caused severe degradation in boiling performance. These factors coupled with the dependence of the plain finned surfaces' nucleate boiling curves on fin length (based on base area; see Fig. 3) prevented the development of an accurate set of nucleate boiling correlations as was possible for the microporous finned surfaces. In addition, the plain surfaces also exhibited less enhancement of CHF from increased subcooling than the microporous surfaces as can be seen by comparing the CHF values in Fig. 13. From these observations/comparisons, it is concluded that the microporous coating provides better and more consistent pool boiling heat transfer performance for finned surfaces.

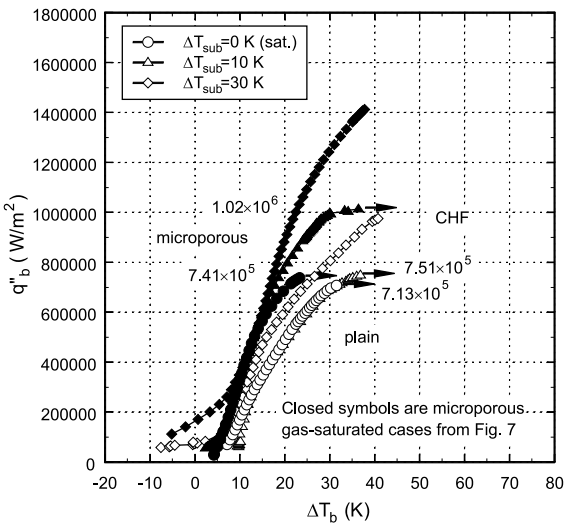

Fig. 13. Comparison of gas-saturated plain and microporous 4 mm finned surfaces at 100 kPa.

4. Conclusions

The effects of pressure, subcooling, and dissolved gas on the pool boiling heat transfer performance of microporous finned (double enhanced) surfaces were investigated along with plain (machine roughened) surfaces for comparison. The copper finned surfaces had base areas of 1-cm^2 (1 cm $\times$ 1 cm) and a 5×5 square pin-fin array with fin lengths of 2, 4 and 8 mm. The test matrix included an absolute pressure range of 30–150 kPa and liquid subcooling levels up to 50 K in FC-72. Following are the major conclusions of this study:

- In general, the effects of pressure and subcooling on the microporous finned surfaces were consistent with the flat surface results of Rainey [14] and the prevailing trends in the literature (nucleate boiling performance increased with increased pressure; negligible subcooling effect), however, increased subcooling appears to delay the formation of the temporal dry-out situation near the base of the fins and shifts the entire upper portion of the boiling curve upward.
- A linear-type correlation, Eq. (4), was found to better fit the present low heat flux region microporous nucleate boiling data than the well-known Rohsenow [24] correlation and was found to correctly predict the effects of pressure for the present range of test conditions. A power-type correlation similar to the one originally proposed by Rainey and You [1] was found to fit the high heat flux region of the present microporous finned surface data. The new correlation, Eq. (6), appears to correctly predict the effects

of both pressure and subcooling on the high heat flux region of the microporous boiling curve.

- The nucleate boiling and CHF performance of the 0° (horizontal base/vertical fins) orientation was found to be slightly better than the 90° (vertical base/horizontal fins) orientation for the present finned heater geometry and may be due to the 90° orientation having a significant portion of the finned surface area facing downward.
- The effect of pressure and subcooling on the microporous finned surface CHF values was also found to be consistent with the flat surface results of Rainey [14] (increased CHF with increased pressure/subcooling). In addition, the saturated microporous CHF values decreased linearly with increasing fin length, which is attributed to decreased fin tip heat transfer effectiveness from reduced fin tip temperatures. The microporous CHF values are well correlated/estimated for pressure, subcooling, and fin length with Eqs. (7)–(10).
- The effects of pressure and subcooling on the plain finned surface nucleate boiling and CHF results were similar to the microporous finned surface results, however, the plain surfaces generally exhibited worse boiling heat transfer performance and less enhancement from increased subcooling than the microporous surfaces and experienced significant degradation in performance from oxidation at high levels of dissolved gas content. Therefore, it was concluded that for pool nucleate boiling applications, the microporous coating significantly improves the boiling heat transfer performance of square, pin-finned surfaces in the range of fluid conditions tested.

Acknowledgements

The Desktop Architecture Lab group of Intel Corporation supported this study. The authors extend their thanks to the 3M Industrial Chemical Products Division for the donation of FC-72 test liquid.

References

[1] K.N. Rainey, S.M. You, Pool boiling heat transfer from plain and microporous square pin, finned surfaces in saturated FC-72, Journal of Heat Transfer 122 (3) (2000) 509–516.

[2] K. Nishikawa, Y. Fujita, H. Ohta, S. Hidaka, Effects of system pressure and surface roughness on nucleate boiling heat transfer, Memoirs of the Faculty of Engineering, Kyushu University 42 (2) (1982) 95–111.

[3] M.T. Cichelli, C.F. Bonilla, Heat transfer to liquids boiling under pressure, AIChE Transactions 41 (6) (1945) 755–787.

[4] V.P. Carey, Liquid–Vapor Phase-Change Phenomena, Taylor and Francis, 1992.

[5] Y. Elkassabgi, J.H. Lienhard, Influences of subcooling on burnout of horizontal cylindrical heaters, Journal of Heat Transfer 110 (1988) 479–486.

[6] Y.S. Hong, C.N. Ammerman, S.M. You, Effects of length scale, subcooling, and dissolved gas content on the pool boiling critical heat flux of cylindrical heaters, in: Proceedings of the 11th International Heat Transfer Conference, Kyongju, Korea, 1998, pp. 389–394.

[7] W.H. McAdams, W.E. Kennel, C.S. Minden, R. Carl, P.M. Picornell, J.E. Dew, Heat transfer at high rates to water with surface boiling, Industrial and Engineering Chemistry 41 (9) (1949) 1945–1953.

[8] A.A. Watwe, A. Bar-Cohen, Nucleate pool boiling and critical heat flux in gas-saturated dielectric coolants, in: Proceedings of the 2nd European Thermal-Sciences and 14th UIT National Heat Transfer Conference, Rome, Italy, 1996, pp. 1631–1638.

[9] N. Abuaf, S.H. Black, F.W. Staub, Pool boiling performance of finned surfaces in R-113, International Journal of Heat and Fluid Flow 6 (1) (1985) 23–30.

[10] G. Guglielmini, M. Misale, C. Schenone, Experiments on pool boiling of a dielectric fluid on extended surfaces, International Communications in Heat and Mass Transfer 23 (4) (1996) 451–462.

[11] W.R. McGillis, V.P. Carey, J.S. Fitch, W.R. Hamburgen, Pool boiling enhancement techniques for water at low pressure, in: Proceedings, Seventh Annual IEEE Semiconductor Thermal Measurement and Management Symposium, IEEE, New York, 1991, pp. 64–72.

[12] N. Zuber, Hydrodynamic aspects of boiling heat transfer, AEC Report no. AECU-4439, Physics and Mathematics, 1959.

[13] I. Mudawar, T.M. Anderson, High flux electronic cooling by means of pool boiling. Part II: optimization of enhanced surface geometry, Heat Transfer in Electronics HTD-111 (1989) 35–49.

[14] K.N. Rainey, Pool and flow boiling heat transfer from microporous flat and finned surfaces in FC-72, Ph.D. thesis, The University of Texas at Arlington, Arlington, TX, 2001.

[15] J.Y. Chang, S.M. You, Enhanced boiling heat transfer from micro-porous surfaces: effects of a coating composition and method, International Journal of Heat and Mass Transfer 40 (18) (1997) 4449–4460.

[16] J.P. O'Connor, S.M. You, A painting technique to enhance pool boiling heat transfer in FC-72, Journal of Heat Transfer 117 (2) (1995) 387–393.

[17] J.Y. Chang, S.M. You, Boiling heat transfer phenomena from micro-porous and porous surfaces in saturated FC-72, International Journal of Heat and Mass Transfer 40 (18) (1997) 4437–4447.

[18] S.M. You, J.P. O'Connor, US Patent no. 5814392, 1998.

[19] Y.S. Hong, C.N. Ammerman, S.M. You, Boiling characteristics of cylindrical heaters in saturated, gas saturated, and pure-subcooled FC-72, Journal of Heat Transfer 119 (1997) 313–318.

[20] S.J. Kline, F.A. McClintock, Describing uncertainties in single-sample experiments, Mechanical Engineering 75 (1) (1953) 3–8.

[21] S.M. You, T.W. Simon, A. Bar-Cohen, Experiments on nucleate boiling heat transfer with a highly-wetting dielectric fluid: effects of pressure, subcooling and dissolved gas content, Cryogenic and Immersion Cooling of Optics and Electronic Equipment HTD-131 (1990) 45–52.

[22] K.N. Rainey, S.M. You, Effects of heater orientation on pool boiling heat transfer from microporous coated surfaces, International Journal of Heat and Mass Transfer 44 (14) (2001) 2589–2599.

[23] S. Kumagai, S.G. Jho, Y. Hirono, R. Shimada, T. Takeyama, Boiling heat transfer from circular surfaces with rectangular fin array, Heat Transfer-Japanese Research 16 (2) (1987) 69–81.

[24] W.M. Rohsenow, A method of correlating heat transfer data for surface boiling of liquids, Journal of Heat Transfer 74 (1962) 969–975.

[25] A.A. Watwe, A. Bar-Cohen, A. McNeil, Combined pressure and subcooling effects on pool boiling from a ppga chip package, Journal of Electronic Packaging 119 (1997) 95–105.

[26] A. Bar-Cohen, A. McNeil, Parametric effects on pool boiling critical heat flux in dielectric liquids, in: Proceedings of the Engineering Foundation Conference on Pool and External Flow Boiling, ASME, Santa Barbara, CA, 1992, pp. 171–175.

[27] A.K. Gorodov, O.N. Kaban'kov, A.T. Komov, V.V. Yagov, Critical boiling heat fluxes to liquids at subatmospheric pressures, Heat Transfer-Soviet Research 11 (3) (1979) 53–61.

[28] T. Inoue, N. Kawae, M. Monde, Effect of subcooling on critical heat flux during pool boiling on a horizontal wire, Heat and Mass Transfer 33 (5–6) (1998) 481–488.